THE JOURNAL OF PHYSICAL CHEMISTRY B

Article

pubs.acs.org/JPCB

N3 Protonation Induces Base Rotation of 2′-Deoxyadenosine-5′-monophosphate and Adenosine-5′-monophosphate

R. R. Wu,[†] C. C. He,[†] L. A. Hamlow,[†] Y.-w. Nei,[†] G. Berden,[‡] J. Oomens,[‡,§] and M. T. Rodgers*[,†]

[†]Department of Chemistry, Wayne State University, Detroit, Michigan 48202, United States

[‡]FELIX Laboratory, Institute for Molecules and Materials, Radboud University, Toernooiveld 7, 6525 ED Nijmegen, The Netherlands

[§]van't Hoff Institute for Molecular Sciences, University of Amsterdam, 1090 GD Amsterdam, The Netherlands

Supporting Information

ABSTRACT: Infrared multiple photon dissociation (IRMPD) action spectroscopy experiments combined with theoretical calculations are performed to investigate the stable gas-phase conformations of the protonated adenine mononucleotides, $[pdAdo+H]^+$ and $[pAdo+H]^+$. Conformations that are present in the experiments are elucidated via comparative analyses of the experimental IRMPD spectra and the B3LYP/6-311+G(d,p) IR spectra predicted for the conformers optimized at this level of theory. N3 protonation is preferred as it induces base rotation, which allows a strong hydrogen bond to be formed between the excess proton of adenine and the phosphate moiety. In contrast, both N1 and N7 protonation are predicted to be >35 kJ/mol less favorable than N3 protonation. Only N3 protonated conformers are present in the experiments in measurable abundance. Both the low-energy conformers computed and the experimental IRMPD spectra of $[pdAdo+H]^+$ and $[pAdo+H]^+$ indicate that the 2′-hydroxyl moiety does not significantly impact the structure of the most stable conformer or the IRMPD spectral profile of $[pAdo+H]^+$ vs that of $[pdAdo+H]^+$. However, the 2′-hydroxyl leads to a 3-fold enhancement in the IRMPD yield of $[pAdo+H]^+$ in the fingerprint region. Comparison of present results to those reported in a previous IRMPD study of the analogous protonated adenine nucleosides allows the effects of the phosphate moiety on the gas-phase conformations to be elucidated.

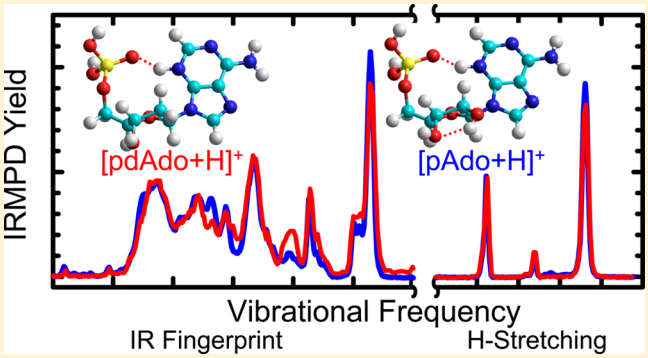

INTRODUCTION

Adenine nucleotides, one of the naturally occurring building blocks of nucleic acids, play important roles in encoding the genetic information required to develop living organisms. Besides their fundamental roles as nucleic acid building blocks, adenine nucleotides also participate in important biological processes such as signal transduction, enzyme regulation, and energy metabolism. For example, adenosine-3′,5′-cyclic-monophosphate (cAMP) facilitates intracellular signal transduction.[1] Flavin adenine dinucleotide and nicotinamide adenine dinucleotide function as coenzymes for biological redox reactions of proteins.[2,3] Intracellular adenosine diphosphate (ADP) and adenosine triphosphate (ATP) participate in biological energy production and transfer reactions,[4] whereas extracellular adenine nucleotides mediate signals through membrane-associated adenosine and ATP receptors.[5] The adenine nucleotides are clearly of great biological significance as illustrated by the fact that more than 15% of all enzymes require ATP or an adenine derivative for proper function.[6] In addition, 9-[2-(phosphonomethoxy)ethyl]adenine, an acyclic adenosine-5′-monophosphate analogue, exhibits selective antiviral activity against herpes simplex viruses and retroviruses.[7,8]

The local environment surrounding adenine nucleotides greatly mediates their structures and functions. For example, the phosphate anions or the electron-rich nitrogen atoms of the adenine nucleobase are likely to interact with metal cations present in living cells.[9−11] Under acidic conditions, adenine becomes protonated and forms A^+·C or A^+·G mispairs instead of canonical A·T pairs.[12] For these reasons, adenine nucleotides have been included in experimental studies designed to examine their biochemical properties and behavior.[13−20] However, investigation of the intrinsic properties of the adenine mononucleotides, 2′-deoxyadenosine-5′-monophosphate (pdAdo) and adenosine-5′-monophosphate (pAdo), are limited.[21−25] Major et al.[17] found that N1 protonation is preferred for ATP as well as five other ATP derivatives by ^{15}N NMR and theoretical calculations. In contrast, Gidden et al.[21] determined that the lowest lying gas-phase conformation of the protonated form of pdAdo exhibits a syn nucleobase orientation, forming a strong hydrogen-bonding interaction between $N3H^+$ and the phosphate moiety, and C2′-endo sugar puckering by gas-phase ion mobility measurements and

Received: April 21, 2016
Published: May 3, 2016

ACS Publications © 2016 American Chemical Society

DOI: 10.1021/acs.jpcb.6b04052
J. Phys. Chem. B 2016, 120, 4616−4624

theoretical calculations. Therefore, more detailed knowledge of the intrinsic properties of pdAdo and pAdo mononucleotides may help improve our current understanding of their conformational preferences and how they change in a low-pH environment, thus explaining differences observed between gas- and condensed-phase studies.

In the current work, the gas-phase conformations of protonated pdAdo and pAdo, $[pdAdo+H]^+$ and $[pAdo+H]^+$, are probed by infrared multiple photon dissociation (IRMPD) action spectroscopy over the ranges of vibrational frequencies extending from ~600 to 1900 and ~3300 to 3800 cm^{-1}. Electronic structure calculations are performed to determine the stable low-energy structures available to these protonated nucleotides and their relative stabilities. Comparison between the measured and the calculated spectra enables elucidation of the low-energy conformations present in the experiments and firmly establishes the site of protonation. In addition, the current work enables comparison between the structures and IRMPD spectra of $[pdAdo+H]^+$ vs $[pAdo+H]^+$ to elucidate the effects of the 2′-hydroxyl on the structure and IR spectra. This work builds on our previous investigations of protonated common as well as modified DNA and RNA nucleosides[26−30] and the deprotonated forms of the canonical DNA and RNA nucleotides[24,25] such that comparisons to this earlier work enable the influence of protonation and the phosphate moiety on the stable gas-phase conformations of the adenine nucleotides to be elucidated.

Previously, Chiavarino et al.[31] and Lanucara et al.[32] employed similar experimental and theoretical approaches to examine the gas-phase conformations of both deprotonated and protonated cAMP, respectively. Comparison of the current work to these studies enables the influence of a canonical vs cyclic phosphate moiety on the gas-phase conformations to be determined. Comparison of the present IRMPD spectroscopy results to the previous ion mobility results for $[pdAdo+H]^+$ reported by Gidden et al.[21] enables the findings of these experimental techniques to be further validated.

EXPERIMENTAL AND COMPUTATIONAL SECTION

Experimental Procedures. IRMPD spectra of $[pdAdo+H]^+$ and $[pAdo+H]^+$ were acquired using a Fourier transform ion cyclotron resonance mass spectrometer (FT-ICR MS).[33−35] A free electron laser (FEL)[36] and independently an OPO/OPA laser set up (OPO) were used to induce photodissociation of $[pdAdo+H]^+$ and $[pAdo+H]^+$. The mononucleotides were purchased from Sigma-Aldrich (Zwijndrecht, The Netherlands). Solutions of 1 mM pdAdo or pAdo and 100 mM acetic acid were prepared in a 50% MeOH:50% H_2O mixture. Direct infusion of the nucleotide solutions (at 5.0 μL/min) into a Micromass "Z-spray" electrospray ionization (ESI) source was achieved using a syringe pump. The ions emanating from the spray were continuously accumulated and trapped in an rf hexapole ion guide for a few seconds to increase sensitivity and make certain that the ions achieve a thermal distribution of internal energies. Ions were transferred to and captured in the ICR cell by pulsed extraction through a quad bender and an rf octopole ion guide.[34] $[pdAdo+H]^+$ and $[pAdo+H]^+$ were mass selected using stored waveform inverse Fourier transform (SWIFT) techniques trapped for >0.3 s before IRMPD activation to ensure that any ions heated in the transfer process cool to room temperature by radiative emission before being continuously irradiated by the FEL for 2.5 s or the OPO for 4 s to give rise to photofragmentation.

Computational Procedures. ChemDraw structures of pdAdo and pAdo are provided in Figure 1. The most favorable

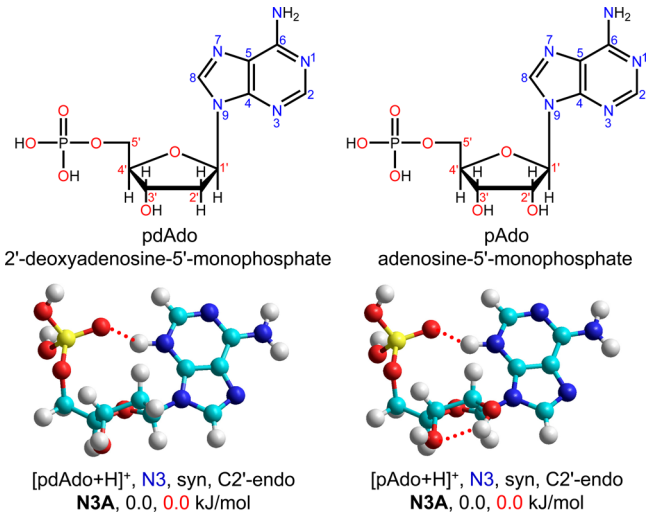

Figure 1. Chemical structures of 2′-deoxyadenosine-5′-monophosphate (pdAdo) and adenosine-5′-monophosphate (pAdo). Ground-state conformers of $[pdAdo+H]^+$ and $[pAdo+H]^+$ predicted at the B3LYP/6-311+G(2d,2p)//B3LYP/6-311+G(d,p) and MP2(full)/6-311+G(2d,2p)//B3LYP/6-311+G(d,p) levels of theory. The preferred site of protonation, nucleobase orientation, and sugar puckering are indicated.

protonation sites, N1, N3, and N7, and the phosphate oxo oxygen atom of $[pdAdo+H]^+$ and $[pAdo+H]^+$ were investigated. Three hundred candidate structures for each site of protonation for both nucleotides were generated from simulated annealing procedures performed using HyperChem software[37] and the Amber 2 force field. Details regarding the simulated annealing process are described in our previous IRMPD studies.[26−28] Calculations including structure optimizations, frequency analyses, and single-point energy determinations for 20−30 favorable candidate structures for each protonation site were performed using Gaussian 09.[38] Candidate structures were initially optimized at the B3LYP/6-31G* level of theory to accelerate convergence and reoptimized using the 6-311+G(d,p) basis set. This procedure has previously been found to provide improved descriptions of the intramolecular hydrogen bonds that stabilize these protonated DNA and RNA nucleosides.[26−30] Linear IR spectra were generated from frequency analyses of the reoptimized structures. Energies of these structures were determined using the 6-311+G(2d,2p) basis set at the B3LYP and MP2(full) levels. The relative stabilities of these structures were determined after including both zero-point energy (ZPE) and thermal corrections to 298 K based on the computed vibrational frequencies. Proposed and empirically determined scaling factors for the vibrational modes from the phosphate moiety vary between 0.98 and 1.07.[24,25,39−48] Therefore, in the calculated spectra of Figures 3 and 4 and Figures S3−S5 of the Supporting Information, a factor of 1.03 is applied to frequencies below ~1350 cm^{-1} (shown in red) to best match the measured phosphate stretching modes. The nucleobase stretching modes, which appear in the ranges of ~1350−1900 and ~3300−3700 cm^{-1}, are scaled by factors of 0.98 (shown in blue) and 0.957 (shown in green), respectively. To best reproduce the measured IRMPD spectral profiles, the predicted

DOI: 10.1021/acs.jpcb.6b04052
J. Phys. Chem. B 2016, 120, 4616−4624

IR spectra are broadened using Gaussian line shapes having a fwhm of 20 cm^{-1} in the IR fingerprint region and 10 cm^{-1} over the hydrogen-stretching region.

RESULTS

IRMPD Action Spectroscopy. Protonated adenine, $[Ade+H]^+$, resulting from cleavage of the glycosidic bond is the only photodissociation product observed for $[pdAdo+H]^+$ and $[pAdo+H]^+$ over both spectral regions. The IRMPD yield was determined from the intensity of the protonated nucleotide, $[pNuo+H]^+$ = $[pdAdo+H]^+$ or $[pAdo+H]^+$, and the intensity of the product ion, $[Ade+H]^+$, produced by laser irradiation at each frequency as shown in the equation below.

$$\text{IRMPD Yield} = \text{Intensity}_{[Ade+H]^+} / (\text{Intensity}_{[Ade+H]^+} + \text{Intensity}_{[pNuo+H]^+}) \quad (1)$$

Corrections to the IRMPD yield associated with the wavelength-dependent output of the FEL and OPO lasers were applied via linear normalization. The IRMPD action spectra recorded for $[pdAdo+H]^+$ and $[pAdo+H]^+$ are displayed in Figure 2. The spectral profiles of $[pdAdo+H]^+$ and $[pAdo+H]^+$ exhibit a high degree of similarity, with only very minor differences in the vibrational frequencies of the spectral features. The influence of the 2′-hydroxyl is primarily reflected in the observed IRMPD yields. In the IR fingerprint region, the IRMPD yield of $[pAdo+H]^+$ is greater than that of $[pdAdo+H]^+$ by a factor of 3, whereas in the hydrogen-stretching region, $[pdAdo+H]^+$ and $[pAdo+H]^+$ exhibit nearly identical IRMPD yields.

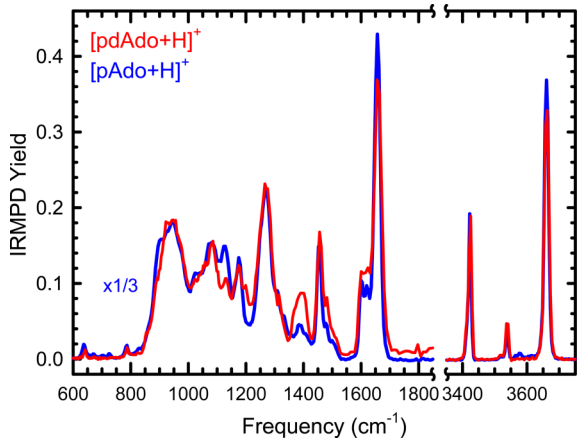

Figure 2. Infrared multiple photon dissociation (IRMPD) action spectra of $[pdAdo+H]^+$ and $[pAdo+H]^+$ in the IR fingerprint and hydrogen-stretching regions. The IRMPD spectrum of $[pAdo+H]^+$ has been multiplied by a factor of 1/3 (only in the IR fingerprint region) to facilitate comparisons.

Theoretical Results. Both the B3LYP and the MP2(full) levels of theory find the same ground-state structures for $[pdAdo+H]^+$ and $[pAdo+H]^+$, which are highly parallel to one another and are shown in Figure 1. N3 is the preferred site of protonation, which induces rotation of the adenine moiety to a syn orientation to form a hydrogen bond with the oxo oxygen atom of the phosphate moiety. Both ground-state structures exhibit C2′-endo sugar puckering. The 2′-hydroxyl substituent of $[pAdo+H]^+$ hydrogen bonds to the adjacent 3′-hydroxyl and leads to a minor change in the rotation of the 3′-hydroxyl as compared to that of $[pdAdo+H]^+$. These findings parallel those found for $[dAdo+H]^+$ and $[Ado+H]^+$.[26] N3 is computed to be the most favorable protonation site for the adenine nucleosides and mononucleotides, which differs from that found for protonated adenine, $[Ade+H]^+$, and protonated ATP, where N1 is preferred.[49,50] Select geometric parameters of the most stable conformers of the protonated adenine nucleotides are compared with those found for the protonated adenine nucleosides[26] in Table 1. The 2′-hydroxyl moiety appears to slightly enhance the strength of the N-glycosidic bond as the C1′−N9 glycosidic bond is shorter for the RNA nucleosides and nucleotides than their DNA analogues. The phosphate moiety of $[pdAdo+H]^+$ and $[pAdo+H]^+$ is a better hydrogen-bond acceptor than the 5′-hydroxyl substituent of the sugar and thus enables a stronger intramolecular hydrogen-bonding interaction with the N3 protonated adenine moiety to be formed, as the $N3H^+\cdots O$ hydrogen bond in the protonated nucleotides is greater than 0.10 Å shorter than in their analogous protonated nucleosides. The phosphate moieties of $[pdAdo+H]^+$ and $[pAdo+H]^+$ also slightly alter the nucleobase orientation, C2′-endo sugar puckering, and the rotation of the 5′-hydroxymethyl substituent relative to the ribosyl moiety as compared to the analogous DNA and RNA nucleosides as reflected by the modest changes in the ∠C4N9C1′C2′, ∠C1′C2′C3′C4′, and ∠O5′C5′C4′O4′ dihedral angles of ∼1−3°, ∼8−14°, and ∼15°, respectively.

The relative enthalpies and free energies (at zero and 298 K) of the stable conformers of $[pdAdo+H]^+$ and $[pAdo+H]^+$ for N3, N1, and N7 sites of protonation are summarized in Table 2. The optimized structures and their 298 K relative free energies of the stable conformers are also compared in the Supporting Information in Figures S1 and S2. The conformers displayed in these figures include all possible combinations of nucleobase orientation and sugar puckering for each favorable site of protonation. No structures protonated at the phosphate oxo oxygen are shown as these structures always converged to N3 protonated species during the optimization process. The nomenclature used to differentiate the low-energy conformers

Table 1. Key Geometrical Parameters of the Ground-State Conformers of the Protonated Forms of the Adenine Nucleosides and Nucleotides

	bond distances (Å)		dihedral angles (deg)		
species	C1′−N9	$N3H^+\cdots O$	∠C4N9C1′C2′	∠C1′C2C3′C4′	∠O5′C5′C4′O4′
$[pdAdo+H]^+$	1.458	1.667	−71.7	−22.2	−75.9
$[pAdo+H]^+$	1.453	1.684	−75.0	−17.2	−75.3
$[dAdo+H]^+$ [a]	1.465	1.801	−72.0	−30.2	−60.4
$[Ado+H]^+$ [a]	1.459	1.830	−71.8	−30.9	−60.3

[a]Values taken from ref 26.

DOI: 10.1021/acs.jpcb.6b04052
J. Phys. Chem. B 2016, 120, 4616−4624

Table 2. Relative Enthalpies and Free Energies of Stable Low-Energy Conformers of $[pdAdo+H]^+$ and $[pAdo+H]^+$ at 0 and 298 K (in kJ/mol)[a]

		B3LYP			MP2(full)		
species	conformer	ΔH_0	ΔH_{298}	ΔG_{298}	ΔH_0	ΔH_{298}	ΔG_{298}
$[pdAdo+H]^+$	**N3A**	**0.0**	**0.0**	**0.0**	**0.0**	**0.0**	**0.0**
	N3B	6.7	6.8	6.7	7.7	7.7	7.7
	N3C	10.5	10.4	11.9	5.9	5.8	7.3
	N3D	22.2	21.4	24.9	10.3	9.4	12.9
	N7A	39.1	41.3	35.2	48.5	50.7	44.6
	N1A	39.4	40.4	37.2	40.8	41.9	38.7
	N3a	43.8	44.4	42.6	46.9	47.6	45.7
	N1B	44.1	44.9	42.9	39.1	39.9	37.8
	N7B	79.1	80.9	75.3	75.8	77.6	72.1
$[pAdo+H]^+$	**N3A**	**0.0**	**0.0**	**0.0**	**0.0**	**0.0**	**0.0**
	N3i	4.8	5.0	5.7	2.2	2.5	3.1
	N3B	8.0	7.7	9.7	7.4	7.1	9.1
	N3ii	12.2	12.2	13.6	10.6	10.6	12.0
	N3C	13.1	13.0	15.0	7.1	7.1	9.0
	N3D	19.9	18.9	24.0	5.0	4.0	9.0
	N3iii	22.5	22.1	25.3	10.1	9.6	12.8
	N1A	37.9	39.0	36.1	38.5	39.6	36.7
	N7A	43.0	44.6	41.7	47.9	49.6	46.7
	N1B	44.3	44.8	44.8	37.6	38.2	38.1
	N7B	78.0	79.4	76.7	73.2	74.6	72.0

[a]Energetics based on single-point energy calculations performed at the B3LYP/6-311+G(2d,2p) and MP2(full)/6-311+G(2d,2p) levels of theory including ZPE and thermal corrections based on the B3LYP/6-311+G(d,p)-optimized structures and vibrational frequencies.

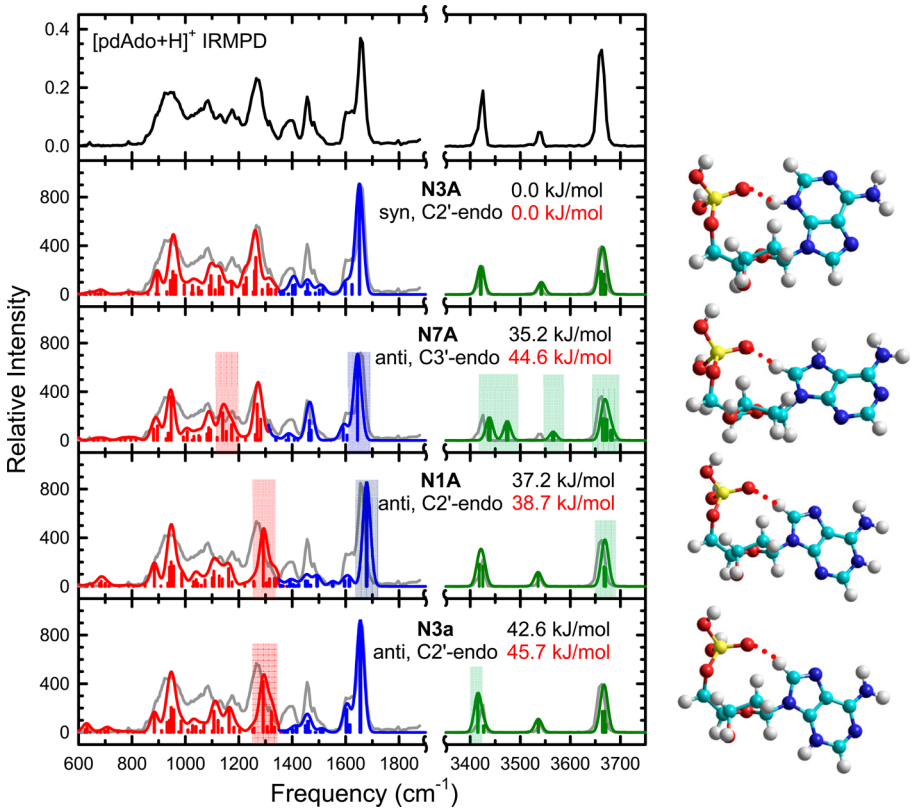

Figure 3. Comparison of the measured IRMPD action spectrum of $[pdAdo+H]^+$ with the calculated IR spectra for the ground-state and representative low-energy conformers of $[pdAdo+H]^+$ for each site of protonation along with the corresponding structures optimized at the B3LYP/6-311+G(d,p) level of theory. Also shown are the B3LYP/6-311+G(2d,2p) (in black) and MP2(full)/6-311+G(2d,2p) (in red) relative Gibbs free energies at 298 K. The site of protonation, nucleobase orientation, and sugar puckering are also indicated for each conformer.

is based on the protonation site and either a capital letter when parallel structures are found for both $[pdAdo+H]^+$ and $[pAdo+H]^+$ (**N3A**, **N3B**, **N3C**, etc.), a lowercase letter for the single conformer (**N3a**) that is found only for $[pdAdo+H]^+$,

DOI: 10.1021/acs.jpcb.6b04052
J. Phys. Chem. B 2016, 120, 4616−4624

or a lowercase Roman numeral for structures (**N3i**, **N3ii**, and **N3iii**) that are found only for $[pAdo+H]^+$. Theory suggests that the N1 and N7 protonated conformers are >35 kJ/mol less favorable than the N3 protonated ground-state conformers.

N3 Protonation. For both $[pdAdo+H]^+$ and $[pAdo+H]^+$, N3 protonation allows the nucleobase to rotate into a syn orientation and form a strong ionic hydrogen-bonding interaction with the phosphate moiety. The relative stabilities of N3 protonated low-energy conformers of $[pdAdo+H]^+$ and $[pAdo+H]^+$ (i.e., **N3A**, **N3B**, **N3i**, and **N3ii**) indicate that puckering of the sugar in a C2′-endo configuration is slightly more stable than C3′-endo. In addition, the relative stabilities of **N3A** and **N3i** and **N3B** and **N3ii** of $[pAdo+H]^+$, respectively, suggest that regardless of the sugar configuration, the structure is found to be more stable when the 2′-hydroxyl serves as a hydrogen-bond donor to the adjacent 3′-hdyroxyl substituent, consistent with that found for the protonated adenine nucleosides.[26] The **N3C** and **N3D** conformers of both $[pdAdo+H]^+$ and $[pAdo+H]^+$ also have the N3 protonated adenine in a syn orientation but are instead hydrogen bonded to O5′ rather than the phosphate oxo oxygen atom, similar to the structure of the protonated nucleosides. These conformers lie at least 10 kJ/mol higher in free energy than the most stable conformers computed, again indicating that the phosphate moiety is a better hydrogen-bond acceptor than the sugar hydroxyls. The **N3a** conformer of $[pdAdo+H]^+$ is >40 kJ/mol less stable than **N3A**, indicating that the $N3H^+\cdots O{=}P$ hydrogen bond strongly stabilizes the syn conformation vs the anti orientation, which is only stabilized by a weak noncanonical hydrogen bond. The anti nucleobase conformer **N3iii** of $[pAdo+H]^+$ is stabilized by $N3H^+\cdots O2'H\cdots O3'$ dual hydrogen bonds enabled by the additional 2′-hydroxyl moiety such that it is only ∼25 kJ/mol less stable than the **N3A** ground-state conformer.

N1 and N7 Protonation. N1 and N7 protonation of both $[pdAdo+H]^+$ and $[pAdo+H]^+$ is computed to be >35 kJ/mol less favorable than the N3 protonated ground-state conformers. B3LYP predicts that N7 is slightly more favorable than N1 for $[pdAdo+H]^+$, whereas MP2(full) prefers N1 over N7 for $[pdAdo+H]^+$. In contrast, both B3LYP and MP2(full) prefer N1 over N7 for $[Ado+H]^+$. The relative stabilities of the N1 and N7 protonated conformers of both $[pdAdo+H]^+$ and $[pAdo+H]^+$ suggest that N1 protonation prefers an anti nucleobase orientation with C2′-endo sugar puckering. N7 protonation also leads to a preference for an anti nucleobase orientation, but with C3′-endo sugar puckering. These observations are again consistent with the structures found for the protonated adenine nucleosides.[26]

DISCUSSION

Elucidation of the Conformers of $[pdAdo+H]^+$ Present in the Experiments. The measured IRMPD and predicted IR spectra of the most stable conformers for each protonation site, **N3A**, **N7A**, and **N1A**, as well as the most stable N3 protonated conformer in which adenine exhibits an anti configuration, **N3a**, of $[pdAdo+H]^+$ are compared over both spectral regions in Figure 3. Mismatches between the measured and the calculated band positions are highlighted to facilitate comparisons. The predicted IR spectrum of the ground-state **N3A** conformer exhibits good agreement with the experimental spectrum in both regions in terms of the band positions, i.e., the resonant vibrational frequencies. However, the relative intensities of several of the bands observed in the IR fingerprint region are not well reproduced by theory, likely due to multiphoton effects in the experiments. Therefore, the syn-oriented **N3A** conformer is present in measurable abundance in the experiments. When the N3 protonated adenine moiety is in an anti orientation, as in the **N3a** conformer, obvious differences between the measured and the predicted spectrum are found. The spectral features predicted at ∼1300 and 3415 cm^{-1} are higher and lower in frequency than the observed bands, which appear at ∼1265 and 3425 cm^{-1}, respectively. Therefore, the anti-oriented **N3a** conformer is unlikely present in appreciable abundance. The strong band calculated at ∼1645 cm^{-1} for **N7A** is of slightly lower frequency than the measured band at ∼1655 cm^{-1}. The calculated band at ∼1150 cm^{-1} for **N7A** lies between the measured bands observed at ∼1175 and 1125 cm^{-1} and would broaden these bands if the **N7A** conformer was present in appreciable abundance. The bands computed for **N7A** at ∼3670, ∼3565, and ∼3438 cm^{-1} are higher in frequency than the measured bands, which are observed at ∼3660, ∼3535, and ∼3425 cm^{-1}, respectively. Moreover, the band at ∼3475 cm^{-1} predicted for **N7A** is not observed in the measured spectrum. The calculated bands at ∼3670, ∼1680, and ∼1290 cm^{-1} for **N1A** are higher in frequency than the measured bands at ∼3660, ∼1655, and ∼1265 cm^{-1}, respectively. Therefore, **N7A** and **N1A**, the most stable N7 and N1 protonated conformers computed, are not present in measurable abundance. Similar comparisons of the measured vs calculated spectra of the **N3B**, **N3C**, **N3D**, **N1B**, and **N7B** conformers of $[pdAdo+H]^+$ are shown in Figure S3 of the Supporting Information. The predicted IR spectra of these five conformers all show differences vs the experimental IRMPD spectrum that indicate that they cannot be significant contributors to the measured IRMPD spectrum. Details are discussed in the Supporting Information.

In summary, the overall similarities as well as the differences between the measured IRMPD and the predicted IR spectra for the stable structures of $[pdAdo+H]^+$ over both IR spectral regions examined clearly indicate that all conformers protonated at either N1 or N7 are not important contributors to the measured spectrum. The agreement between the measured and the calculated spectra for the ground-state **N3A** conformer, which exhibits a syn nucleobase orientation and C2′-endo puckering, is very good. Discrepancies between the experimetal and the predicted spectra for the anti-oriented **N3a** conformer also suggest that this conformer cannot be present in significant abundance. The calculated IR spectrum of **N3A** allows the measured IRMPD spectrum to be interpreted. Assignments of the vibrational modes of $[pdAdo+H]^+$ are summarized in Table 3.

Elucidation of the Conformers of $[pAdo+H]^+$ Present in the Experiments. The measured IRMPD and IR spectra predicted for the most stable conformers for each protonation site examined, **N3A**, **N1A**, and **N7A**, as well as the most stable N3 protonated conformer in which adenine exhibits an anti configuration, **N3iii**, of $[pAdo+H]^+$ are compared over both spectral regions in Figure 4. Mismatches between the measured and the predicted band positions are again highlighted to facilitate comparisons. The calculated spectrum of the ground-state **N3A** conformer exhibits good spectral alignment with the experimental spectrum in both regions except for the absence in the measured spectrum of the weak IR feature predicted at 3685 cm^{-1}. As found for $[pdAdo+H]^+$, the relative intensities of several of the bands observed in the IR fingerprint region are not well reproduced by theory, which is again attributed to

DOI: 10.1021/acs.jpcb.6b04052
J. Phys. Chem. B 2016, 120, 4616−4624

Table 3. Vibrational Mode Assignments of $[pdAdo+H]^+$ and $[pAdo+H]^+$ [a]

vibrational mode assignment	frequency (cm^{-1}) $[pdAdo+H]^+$	$[pAdo+H]^+$
P−OH bending	935	938
sugar ring stretching	1075	1071
C5′−O5′ stretching	1124	1123
C4′−C5′ stretching	1171	1175
P═O stretching	1266	1263
sugar hydrogen bending	1390	1385
N1═C6 and C8−N9 stretching	1456	1452
N3−C4 and N1−C2 stretching	1608	1610
NH_2 scissoring	1656	1657
NH_2 symmetric stretching	3425	3422
NH_2 asymmetric stretching	3536	3538
O2′H stretching		3567
P−OH and O3′H stretching	3662	3661

[a]Vibrational assignments based on comparison of the measured IRMPD and calculated IR spectra of the ground-state **N3A** conformers of $[pdAdo+H]^+$ and $[pAdo+H]^+$.

multiphoton effects in the experiments. The predicted feature at 3685 cm^{-1} is associated with O3′H stretching. The strong intramolecular hydrogen-bonding interaction between 2′- and 3′-hydroxyls may lead to a blue shift in the predicted feature vs the band position measured (3662 cm^{-1}). Notice that the 3′-hydroxyl also serves as a hydrogen-bond acceptor in the **N3iii**, **N1A**, and **N7A** conformers shown in Figure 4. As found for the **N3A** conformer, the vibrational frequencies of the O3′H stretches of these conformers are overpredicted. Therefore, the shift of the predicted hydrogen-bond acceptor O3′H stretch relative to the measured band may not be diagnostically useful. The calculated bands at ~1680 cm^{-1} for **N1A** and ~1295 cm^{-1} for both **N3iii** and **N1A** are higher in frequency than the bands recorded at ~1655 and ~1265 cm^{-1}, respectively. The broad bands predicted at ~1140 and ~1150 cm^{-1} for **N3iii** and **N7A**, respectively, are shifted from the observed bands at ~1175 and ~1125 cm^{-1} and would broaden these two bands if **N3iii** and **N7A** were present in appreciable abundance in the experiments. The strong band at ~1645 cm^{-1} for **N7A** is underpredicted by 10 cm^{-1} as the observed band appears at ~1655 cm^{-1}. In addition, the calculated IR spectrum for **N7A** exhibits obvious discrepancies in the hydrogen-stretching region. In particular, the bands at ~3590, ~3565, and ~3440 cm^{-1} are overpredicted as the bands are observed at ~3570, ~3540 and ~3420 cm^{-1}, respectively. The calculated band at ~3470 cm^{-1} is not apparent in the experimental spectrum. Thus, the ground-state **N3A** conformer is clearly contributing to the experimental spectrum, whereas discrepancies between the measured and the calculated spectra indicate that the **N3iii**, **N1A**, and **N7A** conformers cannot be present in appreciable abundance in the experiments. Analogous comparisons for the other low-energy conformers of $[pAdo+H]^+$ are provided in Figures S4 and S5 of the Supporting Information. The IR spectra predicted for all of these conformers show differences vs the experimental spectrum that indicate that they cannot be

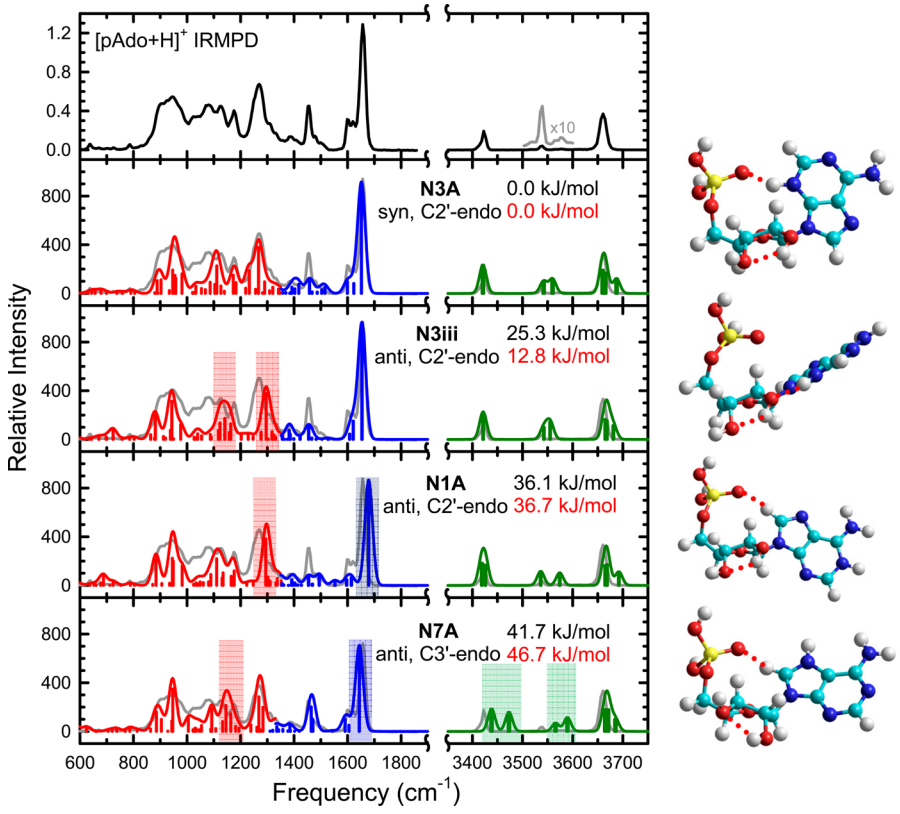

Figure 4. Comparison of the measured IRMPD action spectrum of $[pAdo+H]^+$ with the calculated IR spectra for the ground-state and representative stable low-energy conformers of $[pAdo+H]^+$ for each site of protonation along with the corresponding structures optimized at the B3LYP/6-311+G(d,p) level of theory. Also shown are the B3LYP/6-311+G(2d,2p) (in black) and MP2(full)/6-311+G(2d,2p) (in red) relative Gibbs free energies at 298 K. The site of protonation, nucleobase orientation, and sugar puckering are also indicated for each conformer.

DOI: 10.1021/acs.jpcb.6b04052
J. Phys. Chem. B 2016, 120, 4616−4624

important contributors in the experiments. Details are discussed in the Supporting Information.

In summary, parallel to that found for $[pdAdo+H]^+$, comparative analyses of the experimental and calculated spectra of $[pAdo+H]^+$ over both IR regions indicate that conformers protonated at either the N1 or the N7 atom are not present in appreciable abundance. The ground-state **N3A** conformer is clearly the dominant contributor. **N3A** exhibits a syn nucleobase orientation and C2′-endo puckering, and the 2′-hydroxyl substituent serves as a hydrogen-bond donor. The experimental IRMPD spectrum is interpreted based on the calculated IR spectrum of **N3A**; vibrational mode assignments for $[pAdo+H]^+$ are summarized in Table 3.

Comparison of $[pdAdo+H]^+$ and $[pAdo+H]^+$. The measured IRMPD band profiles of $[pdAdo+H]^+$ and $[pAdo+H]^+$ displayed in Figure 2 are remarkably similar. Therefore, it is not surprising that the vibrational modes summarized in Table 3 are nearly identical for $[pdAdo+H]^+$ and $[pAdo+H]^+$ except for the additional broad feature at 3567 cm^{-1} for $[pAdo+H]^+$, which represents O2′H stretching. The differences between the experimental spectra of $[pdAdo+H]^+$ and $[pAdo+H]^+$ primarily lie in the IRMPD band intensities in the FELIX region. Excluding the bands observed at ∼1125 and ∼1390 cm^{-1}, the IRMPD yield of $[pAdo+H]^+$ is roughly three times that of $[pdAdo+H]^+$. This large change in the IRMPD yield suggests that the hydrogen-bonding interactions enabled by the 2′-hydroxyl substituent stiffen the sugar moiety, which allows the nucleobase and phosphate moieties greater flexibility such that the intramolecular vibrational redistribution (IVR)[51,52] is more efficient than for $[pdAdo+H]^+$. No significant differences in the IR intensities of $[pdAdo+H]^+$ and $[pAdo+H]^+$ are theoretically predicted for the features at ∼1125 and ∼1390 cm^{-1}, which again suggests that they arise from multiphoton effects in the experiments.

Influence of the Phosphate Moiety on Gas-Phase Conformation. Our earlier IRMPD study of $[dAdo+H]^+$ and $[Ado+H]^+$[26] found that both N3 and N1 protonated low-energy conformers are present in the experiments and that N3 conformers are dominant. Further, both syn- and anti-oriented N3 protonated conformers of $[dAdo+H]^+$ contribute to the experimental spectrum, whereas only N3 protonated conformers of $[Ado+H]^+$ having a syn nucleobase orientation appear to contribute. Both C2′-endo and C3′-endo sugar puckering are observed among the N3 protonated conformers present. The N1 protonated conformers that contribute to the measured spectrum exclusively exhibit an anti nucleobase orientation with C2′-endo puckering. In contrast, the present work indicates that the ground-state **N3A** conformers of $[pdAdo+H]^+$ and $[pAdo+H]^+$ are clearly dominant in the experiments. Both ground-state conformers exhibit C2′-endo sugar puckering and are stabilized by a $N3H^+\cdots O{=}P$ hydrogen bond between the syn-oriented nucleobase and phosphate moieties. Clearly, the $N3H^+\cdots O{=}P$ hydrogen bond with the phosphate moiety provides greater intramolecular stabilization to the protonated adenine nucleotides than the $N3H^+\cdots O5'$ hydrogen bond provides to the protonated adenine nucleosides. Therefore, the most stable conformers of $[pdAdo+H]^+$ and $[pAdo+H]^+$ are less flexible than those of $[dAdo+H]^+$ and $[Ado+H]^+$ such that the nucleobase and sugar moieties of $[pdAdo+H]^+$ and $[pAdo+H]^+$ are more effectively locked down.

Influence of Protonation on Gas-Phase Conformation. Our previous IRMPD studies of $[pdAdo-H]^-$ and $[pAdo-H]^-$ found that deprotonation occurs at the phosphate backbone, adenine is found in an anti orientation, and the structures exhibit C3′-endo sugar puckering.[24,25] As compared to $[pdAdo+H]^+$ and $[pAdo+H]^+$, the state of protonation of both the phosphate and the adenine moieties is altered. Thus, it should come as no surprise that protonation significantly influences the gas-phase conformations. The nucleobase orientation changes from anti to syn to stabilize the excess proton via an $N3H^+\cdots O{=}P$ hydrogen-bonding interaction resulting in a more compact structure. The protonation-induced rotation of the base also impacts the puckering of the ribose moiety, which switches from C3′-endo to C2′-endo. These differences suggest that pH changes or differences in the availability of hydrogen-bond donors and acceptors in complex biological environments likely provide a mechanism for base rotation of adenine residues.

Influence of Canonical vs Cyclic Phosphate Moiety on Gas-Phase Conformation. The gas-phase conformations for $[cAMP-H]^-$[31] and $[cAMP+H]^+$[32] were also examined using IRMPD spectroscopy and theoretical calculations. Chiavarino et al.[31] found that the most stable conformer for $[cAMP-H]^-$ exhibits an anti nucleobase orientation and C3′-endo sugar puckering, parallel to that found for $[pdAdo-H]^-$[24] and $[pAdo-H]^-$.[25] In particular, in the ground-state conformer of $[cAMP-H]^-$, an O2′H···O3′ hydrogen-bonding interaction is formed that stabilizes C3′-endo puckering, whereas in $[pdAdo-H]^-$ and $[pAdo-H]^-$, the 3′-OH strongly interacts with the negatively charged oxygen of the phosphate moiety, forming $O3'H\cdots O^-$ and $O2'H\cdots O3'H\cdots O^-$ interactions, respectively, that also stabilize C3′-endo sugar puckering. For $[cAMP+H]^+$, Lanucara et al.[32] found that both N3 and N1 protonated conformers contribute to the population. Both conformers exhibit a syn nucleobase orientation. However, only the N3 protonated conformer can achieve additional stabilization via an $N3H^+\cdots O4'$ hydrogen bond. Cyclization of the phosphate moiety constrains its flexibility such that it is unable to rotate into a position that can support formation of a strong hydrogen bond with the nucleobase. Thus, N1 protonation is now competitive with N3 for cAMP. N3 protonated $[cAMP+H]^+$ prefers C3′-endo sugar puckering, whereas N1 protonation exhibits a preference for C2′-endo sugar puckering.

Comparison to Ion Mobility Results. Previously, Gidden et al.[21] employed ion mobility and theoretical calculations to examine the gas-phase conformation of $[pdAdo+H]^+$. Their results are consistent with the present findings that the most stable conformer is protonated at N3, stabilized by a $N3H^+\cdots O{=}P$ intramolecular hydrogen bond, and exhibits C2′-endo puckering of the ribosyl moiety. The excellent agreement with the ion mobility results validates both experimental determinations and provides greater confidence in the analysis and interpretation of the IR vs IRMPD spectra.

■ CONCLUSIONS

IRMPD spectra of the protonated DNA and RNA adenine nucleotides, $[pdAdo+H]^+$ and $[pAdo+H]^+$, have been acquired and compared to the B3LYP/6-311+G(d,p) IR spectra predicted for the low-energy conformations optimized at the same level. The relative free energies of the various stable conformations of $[pdAdo+H]^+$ and $[pAdo+H]^+$ found indicate a strong preference for N3 protonation. Comparative analyses of the experimental nonlinear IRMPD and computed linear IR spectra of both $[pdAdo+H]^+$ and $[pAdo+H]^+$ clearly indicate that the most stable N3 protonated conformers, **N3A**, are the

DOI: 10.1021/acs.jpcb.6b04052
J. Phys. Chem. B 2016, 120, 4616−4624

dominant contributors to the experimental population. The **N3A** conformers of $[pdAdo+H]^+$ and $[pAdo+H]^+$ are highly parallel as the 2′-hydroxyl moiety does not greatly impact the stable structures. The **N3A** conformers adopt a syn nucleobase orientation, which is favored due to the strong ionic hydrogen bond between the excess proton and the phosphate moiety ($N3H^+\cdots O{=}P$) that is possible for these conformers and C2′-endo sugar puckering. The hydrogen bond between the 2′- and the 3′-hydroxyls of $[pAdo+H]^+$ leads to greater flexibility of the nucleobase and phosphate moieties and more efficient IVR. Therefore, the 2′-hydroxyl moiety produces a 3-fold enhancement in the IRMPD yield of $[pAdo+H]^+$ in the FELIX region vs that of $[pdAdo+H]^+$. Only weak noncanonical hydrogen bonds between the nucleobase and the phosphate moieties are found in the N1 and N7 protonated conformers, and as a result these conformers are predicted to be >35 kJ/mol less favorable than the **N3A** conformers. Significant differences in the measured IRMPD and IR spectra predicted for the N1 and N7 protonated conformers indicate that these conformers cannot be present in appreciable abundance. Comparisons to the previous IRMPD study of $[dAdo+H]^+$ and $[Ado+H]^+$ [26] indicate that the phosphate moiety provides stronger stabilization to the protonated nucleobase such that only the **N3A** conformers of $[pdAdo+H]^+$ and $[pAdo+H]^+$ are present in appreciable abundance in the experiments. This contrasts that found for the protonated adenine nucleosides, where several N3 and N1 protonated conformers are found to coexist in measurable abundance. Combined, these investigations clearly establish that N3 protonation induces base rotation as the protonated adenine moiety is able to stabilize the excess charge via a strong ionic intramolecular hydrogen-bonding interaction that leads to a syn nucleobase orientation.

■ ASSOCIATED CONTENT

Supporting Information

The Supporting Information is available free of charge on the ACS Publications website at DOI: 10.1021/acs.jpcb.6b04052.

Complete citation for ref 38; figures that compare B3LYP/6-311+G(d,p)-optimized stable conformers of $[pdAdo+H]^+$ and $[pAdo+H]^+$ and their B3LYP and MP2(full) relative free energies at 298 K calculated using the 6-311+G(2d,2p) basis set, the measured IRMPD spectra, and calculated linear IR spectra of select conformers of $[pdAdo+H]^+$ and $[pAdo+H]^+$ (PDF)

■ AUTHOR INFORMATION

Corresponding Author

*Phone: 313 577-2431. E-mail: mrodgers@chem.wayne.edu.

Notes

The authors declare no competing financial interest.

■ ACKNOWLEDGMENTS

This work was supported by the National Science Foundation, Grants OISE-0730072, OISE-1357787, and CHE-1409420. Additional support for R.R.W. was provided by Thomas C. Rumble Graduate and Dissertation Fellowships at WSU. WSU C&IT is gratefully acknowledged for computational resources and support. This work was part of the research program of FOM, which is financially supported by the Nederlandse Organisatie voor Wetenschappeklijk Onderzoek. The technical support provided by J.D. Steill and the FELIX staff is gratefully acknowledged.

■ REFERENCES

(1) Dodge-Kafka, K. L.; Kapiloff, M. S. The mAKAP Signaling Complex: Integration of cAMP, Calcium, and MAP Kinase Signaling Pathways. *Eur. J. Cell Biol.* **2006**, *85*, 593−602.

(2) Tu, B. P.; Weissman, J. S. Oxidative Protein Folding in Eukaryotes: Mechanisms and Consequences. *J. Cell Biol.* **2004**, *164*, 341−346.

(3) Belenky, P.; Bogan, K. L.; Brenner, C. NAD^+ Metabolism in Health and Disease. *Trends Biochem. Sci.* **2007**, *32*, 12−19.

(4) Knowles, J. R. The Mechanism of Biotin-Dependent Enzymes. *Annu. Rev. Biochem.* **1989**, *58*, 195−221.

(5) Fredholm, B. B.; Arslan, G.; Halldner, L.; Kull, B.; Schulte, G.; Wasserman, W. Structure and Function of Adenosine Receptors and Their Genes. *Naunyn-Schmiedeberg's Arch. Pharmacol.* **2000**, *362*, 364−374.

(6) Leonard, N. J. Dimensional Probes of Enzyme-Coenzyme Binding-Sites. *Acc. Chem. Res.* **1982**, *15*, 128−135.

(7) Tsai, C.-C.; Follis, K. E.; Sabo, A.; Beck, T. W.; Grant, R. F.; Bischofberger, N.; Benveniste, R. E.; Black, R. Prevention of SIV Infection in Macaques by (*R*)-9-(2-Phosphonylmethoxypropyl)-Adenine. *Science* **1995**, *270*, 1197−1199.

(8) Blindauer, C. A.; Holy, A.; Dvorakova, H.; Sigel, H. Solution Properties of Antiviral Adenine-Nucleotide Analogues. The Acid-Base Properties of 9-[2-(phosphonomethoxy)ethyl]Adenine (PMEA) and of Its N1, N3 and N7 Deaza Derivatives in Aqueous Solution. *J. Chem. Soc., Perkin Trans. 2* **1997**, 2353−2363.

(9) Granot, J.; Fiat, D. Proton Magnetic-Resonance Study of Divalent Metal-Ions Binding to Adenosine 5-Triphosphate. *J. Am. Chem. Soc.* **1977**, *99*, 70−79.

(10) Sigel, R. K. O.; Song, B.; Sigel, H. Stabilities and Structures of Metal Ion Complexes of Adenosine 5′-*O*-Thiomonophosphate ($AMPS^{2-}$) in Comparison with Those of Its Parent Nucleotide (AMP^{2-}) in Aqueous Solution. *J. Am. Chem. Soc.* **1997**, *119*, 744−755.

(11) Lomozik, L.; Gasowska, A. Complexes of Copper (II) with Spermine and Non-covalent Interactions in the Systems Including Nucleosides or Nucleotides. *J. Inorg. Biochem.* **1998**, *72*, 37−47.

(12) Sniden, R. R. *DNA Structure and Function*; Academic Press: San Diego, 1994; pp 15−22.

(13) Summerfield, G. P.; Keenan, J. P.; Brodie, N. J.; Bellingham, A. J. Bioluminescent Assay of Adenine-Nucleotides − Rapid Analysis of ATP and ADP in Red-Cells and Platelets Using the LKB Luminometer. *Clin. Lab. Haematol.* **1981**, *3*, 257−271.

(14) Lunardi, J.; Satre, M.; Vignais, P. V. Exploration of Adenosine 5′-Diphosphate-Adenosine 5′-Triphosphate Binding Sites of Escherichia Coli Adenosine 5′-Triphosphatase with Arylazido Adenine Nucleotides. *Biochemistry* **1981**, *20*, 473−480.

(15) Tribolet, R.; Sigel, H. Self-Association and Protonation of Adenosine 5′-Monophosphate in Comparison with Its 2′- and 3′-Analogues and Tubercidin 5′-Monophosphate (7-Deaza-AMP). *Eur. J. Biochem.* **1987**, *163*, 353−363.

(16) Wang, P.; Izatt, R. M.; Oscarson, J. L.; Gillespie, S. E. ^1H NMR Study of Protonation and Mg(II) Coordination of AMP, ADP and ATP at 25, 50 and 70 °C. *J. Phys. Chem.* **1996**, *100*, 9556−9560.

(17) Major, D. T.; Laxer, A.; Fischer, B. Protonation Studies of Modified Adenine and Adenine Nucleotides by Theoretical Calculations and ^{15}N NMR. *J. Org. Chem.* **2002**, *67*, 790−802.

(18) Marques, I.; Fonrodona, G.; Baro, A.; Guiteras, J.; Beltran, J. L. Study of Solvent Effects on the Acid-Base Behaviour of Adenine, Adenosine 3′,5′-Cyclic Monophosphate and Poly(adenylic) Acid in Acetonitrile-Water Mixtures Using Hard-Modelling and Soft-Modelling Approaches. *Anal. Chim. Acta* **2002**, *471*, 145−158.

(19) Crestoni, M. E.; Fornarini, S. Gas-Phase Hydrogen/Deuterium Exchange of Adenine Nucleotides. *J. Mass Spectrom.* **2003**, *38*, 854−861.

(20) Arranz-Mascaros, P.; Bazzicalupi, C.; Bianchi, A.; Giorgi, C.; Godino-Salido, M. L.; Gutierrez-Valero, M. D.; Lopez-Garzon, R.; Valtancoli, B. Binding and Recognition of AMP, ADP, ATP and Related Inorganic Phosphate Anions by a Tren-Based Ligand

DOI: 10.1021/acs.jpcb.6b04052
J. Phys. Chem. B 2016, 120, 4616−4624

Containing a Pyrimidine Functionality. *New J. Chem.* **2011**, *35*, 1883−1891.
(21) Gidden, J.; Bowers, M. T. Gas-Phase Conformations of Deprotonated and Protonated Mononucleotides Determined By Ion Mobility and Theoretical Modeling. *J. Phys. Chem. B* **2003**, *107*, 12829−12837.
(22) Liu, D.; Wyttenbach, T.; Bowers, M. T. Hydration of Mononucleotides. *J. Am. Chem. Soc.* **2006**, *128*, 15155−15163.
(23) Pedersen, S. O.; Stochkel, K.; Byskov, C. S.; Baggesen, L. M.; Nielsen, S. B. Gas-Phase Spectroscopy of Protonated Adenine, Adenosine 5′-Monophosphate and Monohydrated Ions. *Phys. Chem. Chem. Phys.* **2013**, *15*, 19748−19752.
(24) Nei, Y.-w.; Hallowita, N.; Steill, J. D.; Oomens, J.; Rodgers, M. T. Infrared Multiple Photon Dissociation Action Spectroscopy of Deprotonated DNA Mononucleotides: Gas-Phase Conformations and Energetics. *J. Phys. Chem. A* **2013**, *117*, 1319−1335.
(25) Nei, Y.-w.; Crampton, K. T.; Berden, G.; Oomens, J.; Rodgers, M. T. Infrared Multiple Photon Dissociation Action Spectroscopy of Deprotonated RNA Mononucleotides: Gas-Phase Conformations and Energetics. *J. Phys. Chem. A* **2013**, *117*, 10634−10649.
(26) Wu, R. R.; Yang, B.; Berden, G.; Oomens, J.; Rodgers, M. T. Gas-Phase Conformations and Energetics of Protonated 2′-Deoxyadenosine and Adenosine: IRMPD Action Spectroscopy and Theoretical Studies. *J. Phys. Chem. B* **2015**, *119*, 2795−2805.
(27) Wu, R. R.; Yang, B.; Frieler, C. E.; Berden, G.; Oomens, J.; Rodgers, M. T. N3 and O2 Protonated Tautomeric Conformations of 2′-Deoxycytidine and Cytidine Coexist in the Gas Phase. *J. Phys. Chem. B* **2015**, *119*, 5773−5784.
(28) Wu, R. R.; Yang, B.; Berden, G.; Oomens, J.; Rodgers, M. T. Gas-Phase Conformations and Energetics of Protonated 2′-Deoxyguanosine and Guanosine: IRMPD Action Spectroscopy and Theoretical Studies. *J. Phys. Chem. B* **2014**, *118*, 14774−14784.
(29) Wu, R. R.; Yang, B.; Berden, G.; Oomens, J.; Rodgers, M. T. Diverse Mixtures of 2,4-Dihydroxy Tautomers and O4 Protonated Conformers of Uridine and 2′-Deoxyuridine Coexist in the Gas Phase. *Phys. Chem. Chem. Phys.* **2015**, *17*, 25978−25988.
(30) Wu, R. R.; Yang, B.; Berden, G.; Oomens, J.; Rodgers, M. T. 2,4-Dihydroxy and O2 Protonated Tautomers of dThd and Thd Coexist in the Gas Phase: Methylation Alters Protonation Preferences vs dUrd and Urd. *J. Am. Soc. Mass Spectrom.* **2016**, *27*, 410−421.
(31) Chiavarino, B.; Crestoni, M. E.; Fornarini, S.; Lanucara, F.; Lemaire, J.; Maitre, P.; Scuderi, D. Infrared Spectroscopy of Isolated Nucleotides 1. The Cyclic 3′,5′-Adenosine Monophosphate Anion. *Int. J. Mass Spectrom.* **2008**, *270*, 111−117.
(32) Lanucara, F.; Crestoni, M. E.; Chiavarino, B.; Fornarini, S.; Hernandez, O.; Scuderi, D.; Maitre, P. Infrared Spectroscopy of Nucleotides in the Gas Phase 2. The Protonated Cyclic 3′,5′-Adenosine Monophosphate. *RSC Adv.* **2013**, *3*, 12711−12720.
(33) Valle, J. J.; Eyler, J. R.; Oomens, J.; Moore, D. T.; van der Meer, A. F. G.; von Helden, G.; Meijer, G.; Hendrickson, C. L.; Marshall, A. G.; Blakney, G. T. Free Electron Laser-Fourier Transform Ion Cyclotron Resonance Mass Spectrometry Facility for Obtaining Infrared Multiphoton Dissociation Spectra of Gaseous Ions. *Rev. Sci. Instrum.* **2005**, *76*, 023103−1−023103−7.
(34) Polfer, N. C.; Oomens, J.; Moore, D. T.; von Helden, G.; Meijer, G.; Dunbar, R. C. Infrared Spectroscopy of Phenylalanine Ag(I) and Zn(II) Complexes in the Gas Phase. *J. Am. Chem. Soc.* **2006**, *128*, 517−525.
(35) Polfer, N. C.; Oomens, J. Reaction Products in Mass Spectrometry Elucidated with Infrared Spectroscopy. *Phys. Chem. Chem. Phys.* **2007**, *9*, 3804−3817.
(36) Oepts, D.; van der Meer, A. F. G.; van Amersfoort, P. W. The Free-Electron-Laser User Facility FELIX. *Infrared Phys. Technol.* **1995**, *36*, 297−308.
(37) *HyperChem Computational Chemistry Software Package*, Version 5.0; Hypercube, Inc.: Gainsville, FL, 1997.
(38) Frisch, M. J.; Trucks, G. W.; Schlegel, H. B.; Scuseria, G. E.; Robb, M. A.; Cheeseman, J. R.; Scalmani, G.; Barone, V.; Mennucci, B.; Petersson, G. A.; et al. *Gaussian 09*, Revision C.01; Gaussian, Inc.: Wallingford, CT, 2009. See Supporting Information for full reference .
(39) Katsyuba, S.; Vandyukova, E. Scaled Quantum Mechanical Computations of Vibrational Spectra of Organoelement Molecules, Containing the Atoms P, S, and Cl. *Chem. Phys. Lett.* **2003**, *377*, 658−662.
(40) Jensen, J. O.; Banerjee, A.; Zeroka, D.; Merrow, C. N.; Gilliam, S. J.; Kirkby, S. J. A Theoretical Study of P_4O_{10}: Vibrational Analysis, Infrared and Raman Spectra. *Spectrochim. Acta, Part A* **2004**, *60*, 1947−1955.
(41) Fales, B. S.; Fujamade, N. O.; Oomens, J.; Rodgers, M. T. Infrared Multiple Photon Dissociation Action Spectroscopy and Theoretical Studies of Triethyl Phosphate Complexes: Effects of Protonation and Sodium Cationization on Structure. *J. Am. Soc. Mass Spectrom.* **2011**, *22*, 1862−1871.
(42) Fales, B. S.; Fujamade, N. O.; Nei, Y.-w.; Oomens, J.; Rodgers, M. T. Infrared Multiple Photon Dissociation Action Spectroscopy of Diethyl Phosphate Complexes: Effects of Protonation and Sodium Cationization on Structure. *J. Am. Soc. Mass Spectrom.* **2011**, *22*, 81−92.
(43) Chiavarino, B.; Crestoni, M. E.; Fornarini, S.; Scuderi, D.; Salpin, J.-Y. Interaction of Cisplatin with 5′-dGMP: A Combined IRMPD and Theoretical Study. *Inorg. Chem.* **2015**, *54*, 3513−3522.
(44) Salpin, J.-Y.; MacAleese, L.; Chirot, F.; Dugourd, P. Structure of the Pb^{2+}−Deprotonated dGMP Complex in the Gas Phase: A Combined MS-MS/IRMPD Spectroscopy/Ion Mobility Study. *Phys. Chem. Chem. Phys.* **2014**, *16*, 14127−14138.
(45) Scuderi, D.; Bakker, J. M.; Durand, S.; Maitre, P.; Sharma, A.; Martens, J. K.; Nicol, E.; Clavaguéra, C.; Ohanessian, G. Structure of Singly Hydrated, Protonated Phospho-Tyrosine. *Int. J. Mass Spectrom.* **2011**, *308*, 338−347.
(46) Salpin, J.-Y.; Gamiette, L.; Tortajada, J.; Besson, T.; Maitre, P. Structure of Pb^{2+}/dCMP and Pb^{2+}/CMP Complexes as Characterized by Tandem Mass Spectrometry and IRMPD Spectroscopy. *Int. J. Mass Spectrom.* **2011**, *304*, 154−164.
(47) Salpin, J.-Y.; Guillaumont, S.; Ortiz, D.; Tortajada, J.; Maitre, P. Direct Evidence for Tautomerization of the Uracil Moiety Within the Pb^{2+}/Uridine-5′-Monophosphate Complex: A Combined Tandem Mass Spectrometry and IRMPD Study. *Inorg. Chem.* **2011**, *50*, 7769−7778.
(48) Scuderi, D.; Correia, C. F.; Balaj, O. P.; Ohanessian, G.; Lemaire, J.; Maitre, P. Structural Characterization by IRMPD Spectroscopy and DFT Calculations of Deprotonated Phosphorylated Amino Acids in the Gas Phase. *ChemPhysChem* **2009**, *10*, 1630−1641.
(49) Russo, N.; Toscano, M.; Grand, A.; Jolibois, F. Protonation of Thymine, Cytosine, Adenine, and Guanine DNA Nucleic Acid Bases: Theoretical Investigation into the Framework of Density Functional Theory. *J. Comput. Chem.* **1998**, *19*, 989−1000.
(50) Tureček, F.; Chen, X. Protonated Adenine: Tautomers, Solvated Clusters, and Dissociation Mechanisms. *J. Am. Soc. Mass Spectrom.* **2005**, *16*, 1713−1726.
(51) Eyler, J. R. Infrared Multiple Photon Dissociation Spectroscopy of Ions in Penning Traps. *Mass Spectrom. Rev.* **2009**, *28*, 448−467.
(52) Oomens, J.; Polfer, N. C. Vibrational Spectroscopy of Bare and Solvated Ionic Complexes of Biological Relevance. *Mass Spectrom. Rev.* **2009**, *28*, 468−494.

DOI: 10.1021/acs.jpcb.6b04052
J. Phys. Chem. B 2016, 120, 4616−4624